REPORT DOCUMENTATION PAGE

Form Approved
OMB No. 0704-0188

1. REPORT DATE *(DD-MM-YYYY)*	2. REPORT TYPE	3. DATES COVERED *(From - To)*
	Technical Papers	

4. TITLE AND SUBTITLE

5a. CONTRACT NUMBER

5b. GRANT NUMBER

5c. PROGRAM ELEMENT NUMBER

6. AUTHOR(S)

5d. PROJECT NUMBER

5e. TASK NUMBER

5f. WORK UNIT NUMBER

7. PERFORMING ORGANIZATION NAME(S) AND ADDRESS(ES)

Air Force Research Laboratory (AFMC)
AFRL/PRS
5 Pollux Drive
Edwards AFB CA 93524-7048

8. PERFORMING ORGANIZATION REPORT

9. SPONSORING / MONITORING AGENCY NAME(S) AND ADDRESS(ES)

Air Force Research Laboratory (AFMC)
AFRL/PRS
5 Pollux Drive
Edwards AFB CA 93524-7048

10. SPONSOR/MONITOR'S ACRONYM(S)

11. SPONSOR/MONITOR'S NUMBER(S)

12. DISTRIBUTION / AVAILABILITY STATEMENT

Approved for public release; distribution unlimited.

TP-FY99-0127

65

ERC # E99-020
✓ Spreadsheet
✓ DTS

MEMORANDUM FOR PRR (Contractor/In-House Publication)

FROM: PROI (TI) (STINFO)

2 June1999

SUBJECT: Authorization for Release of Technical Information, Control Number: AFRL-PR-ED-TP-FY99-0127
Spanjers, Schilling, Engelman and Bromaghim, AIAA-99-2709, "In-Flight Contamination Measurements of the ESEX 26 kW Ammonia Arcjet"
AIAA Joint Propulsion Conference **(Public Release)**

15. SUBJECT TERMS

16. SECURITY CLASSIFICATION OF:			17. LIMITATION OF ABSTRACT	18. NUMBER OF PAGES	19a. NAME OF RESPONSIBLE PERSON
a. REPORT	b. ABSTRACT	c. THIS PAGE			Leilani Richardson
Unclassified	Unclassified	Unclassified	A		19b. TELEPHONE NUMBER *(include area code)* (661) 275-5015

41 items enclosed

AIAA-99-2709
In-Flight Contamination Measurements of the ESEX 26 kW Ammonia Arcjet

G.G. Spanjers, J.H. Schilling[1], S.F. Engelman[2], D.B. Bromaghim
Air Force Research Laboratory
Edwards AFB, CA

L.K. Johnson
The Aerospace Corporation
El Segundo, CA

1. Sparta Inc., Air Force Research Laboratory, Edwards AFB, CA
2. ERC Inc, Air Force Research Laboratory, Edwards AFB, CA

35th AIAA/ASME/SAE/ASSEE Joint Propulsion Conference & Exhibit
20-23 June 1999
Los Angeles, California

In-Flight Contamination Measurements of the ESEX 26 kW Ammonia Arcjet

G.G. Spanjers*, J.H. Schilling†, S.F. Engelman‡, D.B. Bromaghim§
Propulsion Directorate, Air Force Research Laboratory, Edwards AFB, CA

L.K. Johnson
The Aerospace Corporation
El Segundo, CA

Abstract

The United States Air Force Research Laboratory's Electric Propulsion Space Experiment (ESEX) was launched and operated in early 1999 in order to demonstrate the compatibility and readiness of a 30-kW class ammonia arcjet for satellite propulsion applications. As part of this flight, an array of on-board contamination sensors was used to assess the effect of the arcjet on the spacecraft surfaces and environment. The contamination sensors have also been used to assess the spacecraft outgassing and to provide information during in-flight anomalies. The sensors consisted of microbalances to measure material deposition, radiometers to assess material degradation due to thermal irradiation, and solar cell segments to quantify the potential for solar array degradation. No material deposition is observed during 6 arcjet firings, with the exception of the first firing. Deposition during the first firing is observed only on the microbalance near the arcjet exit, and is attributed to the expulsion of foreign material within the arcjet that presumably accumulated during the fabrication, integration, and storage of the device prior to launch. Solar cell degradation is observed during the firings and is attributed to the exhaust plasma forming slightly conductive paths away from the cell load. Once the firing ends, the solar cell returns to full operation with no observable degradation. Initial evaluation of the radiometer data suggests some material degradation of the S13-GLO coating, however a more detailed transient analysis is required for a conclusive result. Flight data is continuing to be collected on all contamination sensors to further quantify changes to the spacecraft atmosphere due to operation of the other 8 experiments aboard the ARGOS spacecraft.

I. Introduction

Operation of thermal control and optical surfaces can be impaired by material deposition on spacecraft surfaces. Solar cell operation can be degraded by the presence of a conductive plasma exhaust. Understanding the coupling of these effects with high-power electric propulsion is of critical importance to the development of the next-generation of large AF space structures. A major goal of the USAF Electric Propulsion Space Experiment (ESEX)[1] Advanced Technology Demonstrator is to explore these issues by measuring the contamination effects of a 30-kW class arcjet in flight. ESEX was launched on 23 February 1999 as 1 of 9 experiments aboard the USAF's Advanced Research and Global Observation Satellite (ARGOS)[2].

---

* Leader, USAF Electric Propulsion Group, Member AIAA
† Project Engineer, Sparta Inc., Air Force Research Laboratory, Edwards AFB, CA, Member AIAA
‡ Project Engineer, ERC Inc., Air Force Research Laboratory, Edwards AFB, CA, Member AIAA
§ Program Manager, Member AIAA

During 8 firings of the ESEX arcjet, no measurable material deposition is observed that is attributable to the steady-state operation of the arcjet. Material is collected on the deposition sensor nearest the thruster exit plane on the first firing, however the lack of similar collection on subsequent firings leads to the conclusion that this material was a one-time efflux indicative of the fabrication and handling, and not indicative of steady-state contamination rates. Deposition sensors not in the line-of-sight of the thruster show essentially zero effects from the firing. Solar cell segments placed near the thruster exhaust show increasing degradation through the experiment, attributable to the exhaust plasma partially shorting the solar cell load. Radiometers placed near the thruster exit suggest material degradation of the sensor material, however similar sensors in the backflow region show no adverse effects.

II. Contamination Sensors

To investigate the spacecraft contamination environment the ESEX flight unit is equipped with 4 Thermoelectric Quartz Crystal Microbalances (TQCMs), 4 Radiometers, and a section of GaAs solar array cells. The sensors are positioned around the ESEX unit as shown in Fig. 1. Specific sensor locations are listed in Table 1. In Table 1, angle=0 horizontal to the thruster exit plane with negative values in the backflow region. Sensor angle=90 if the sensor normal is directed towards the thruster exit.

A. Thermoelectric Quartz Crystal Microbalances (TQCMs)

The TQCMs are used to convert deposition mass into a frequency change of an oscillating quartz sensor crystal. By measuring the frequency change the mass of material deposits can be determined with a high degree of accuracy. The four ESEX TQCMs are the MK-10 model from QCM Research and were chosen to be identical to those used on the Midcourse Space Experiment (MSX) Satellite[3] launched April 24, 1996. This enabled significant cost-savings by allowing ESEX to take advantage of the characterization and calibration work performed by the MSX team prior to flight[4]. The only difference between the TQCMs on MSX and ESEX is that the MSX used a 15 MHz crystal whereas some clown apparently switched the ESEX sensors to the 10 MHz types for no apparent reason. 15 MHz sensors have higher sensitivity to mass deposition.

As shown in Fig. 1, TQCM #1 is positioned on the witness tower, adjacent to radiometer #1 and at the same height as the thruster exit plane. TQCM #2 is located on the diagnostic deck below the thermal shield. TQCM #3 is located near the edge of the diagnostic deck and has a view of the arcjet plume. TQCM #4 is mounted on the deployable boom that also contains the EMI antenna. For the beginning of the flight the boom was stowed and TQCM #4 faced the spacecraft surface. On Julian day 68.6, the boom was deployed. TQCM #4 then faced the RAM direction of the spacecraft.

The ESEX TQCMs use a 10 MHz crystal sensor resulting in a signal response of 4.49×10^{-9} grams/cm^2/Hz. For a hypothetical contaminant density of 1 gm/cm^3, this corresponds to a deposition thickness of 0.44a angstroms/Hz. The sensor accuracy is 0.2 Hz according to QCM Research[5] and 4 MHz according to the characterization performed for MSX[4]. The higher MSX uncertainty was due to a cyclic variation in the sensor frequency observed during 21-day drift tests. For the ESEX data, the 4 Hz uncertainty is appropriate for long-term measurements of contaminants due to effects such as spacecraft outgassing. The lower 0.2 Hz uncertainty is

appropriate for short duration events such as the sensor response to a 0-15 minute arcjet firing. Frequency response is on the order of microseconds and not an issue for the ESEX measurements.

Exposure of the TQCM crystals to radiation from the sun or the arcjet firing affects the frequency of oscillation by creating a temperature gradient across the crystal diameter. The effect is temporary, with the TQCM returning to the original frequency when the radiation source is removed. From an operations perspective, this *insolation* effect causes the TQCM data to be oscillatory with a frequency dependent on the orbital solar cycle and an amplitude dependent on the specific solar flux at each sensor. An example is shown in Fig.3 where the frequency for TQCM #1 is plotted over 2 days. The solar flux causes an oscillation amplitude of about 200 Hz while mass condensation on the sensor face causes the slow 30 Hz rise observed over the 2 days. The amplitude of the solar oscillation for TQCM sensors 2, 3, and 4 is approximately 160 Hz, 130 Hz, and 160 Hz, respectively. The frequency change due to mass deposition can be deconvoluted from the insolation oscillations by either subtracting the solar oscillation effects or by using data from the same relative time during each orbit. For this initial analysis, we use either the later technique, or simply show the full oscillation.

The TQCMs have the nominal capability to achieve temperatures between 193K and 353K, strongly dependent on the heat sink temperatures. Preflight ESEX thermal analysis indicated that temperatures as low as 173K may be realizable on-orbit for sensors 2 and 3. During the ESEX flight a minimum temperature of 193K was achieved on all 4 sensors, however it could not be maintained through the solar cycle resulting in a temperature oscillation. A 210K temperature was found to be maintainable through the solar cycle. To reduce the potential for temperature oscillations during an arcjet firing, where the TQCM heat sink may be subjected to additional thermal flux, the TQCM sensor temperature was adjusted to 218K and maintained through the ESEX experiment. The TQCM sensors are baked-off by increasing the temperature so as to vaporize some of the condensed material. By comparing the temperature at which the deposited mass is reduced to vapor pressure curves of the candidate specie, the composition of the deposited material can be determined. A total of five bake-offs at temperatures of 298K and 322K have been performed to date. At least one more bake-off will be conducted prior to the ESEX contamination being turned off. A thermographic analysis of the bake-off data has not as yet been performed and will be presented in a later paper.

B. Solar Cells Segments

The effect of arcjet operation on the performance of solar arrays is a matter of obvious concern. To address this issue, two small solar arrays are mounted on top of the ESEX diagnostic tower. Each array consists of four gallium arsenide solar cells wired in series, under a cerium-doped borosilicate cover glass. The arrays are mounted at a 45 degree angle to allow direct exposure to both incident sunlight and to the arcjet plume. One solar array is connected to an open-circuit voltage sensor, the other to a short-circuit current sensor, allowing independant measurement of both parameters. A thermocouple is mounted to the base of the solar array assembly to monitor solar array temperature.

Under direct solar illumination and at temperatures expected for on-orbit operation, the GaAs solar cell arrays are expected to produce a current of XXX mA and a voltage of 4.X V. Unfortunately, due to an oversight in the design phase, the sensing circuit for the open-circuit voltage cannot read values greater than 4.2 volts, so the observed data will be truncated at that value during periods of direct illumination.

C. Radiometers

The ESEX diagnostic package includes four radiometers intended to measure the radiated heat flux at various locations. These sensors consist of titanium witness plates supported by a narrow titanium strut and

an insulating nylon bushing. A reflective aluminum housing surrounds the entire assembly save for an aperture on the front face. By minimizing any heat transfer path other than conduction through the titanium strut and radiation to and from the witness plate, the radiant heat flux at the surface can be calculated from the temperature difference between the plate and the sensor base, given the known thermal conductivity of the strut, bushing, and interfaces. The radiometer face is coated with S13-GLO white paint with an emissivity of approximately 0.25 in the visible range increasing to 0.85 in the infrared.

Radiometer #1 is located on the diagnostic tower immediately below the solar cell experiment, where it has a direct view of the arcjet anode from the shortest possible distance. Radiometer #2 is also located on the diagnostic tower, but below the arcjet heat shield. It is still partially exposed to radiation from the arcjet anode. Radiometer #3 is located on the deck of the diagnostic platform, below the arcjet heat shield. Radiometer #4 is located near the perimeter of the diagnostic platform, with a clear field of view including the entire arcjet system. The locations of all four radiometers are indicated in Fig. 1.

Though intended primarily to measure radiated heat flux from the arcjet, the radiometers also serve to measure the effects of exposure to the arcjet environment on the optical properties of the S13-GLO paint. With the spacecraft in eclipse, the heat balance of the radiometers will be dominated by infrared emission from the sensor head, and the temperature difference between the sensor head and base will be strongly dependant on the IR emissivity of the surface material. In direct sunlight, the heat balance is dominated by solar absorbtivity. Observation of the long-term radiometer behavior before and after arcjet firings may show changes in IR or visible (solar) emissivity due to degradation of the paint due to exposure to the arcjet environment.

III. Flight Data

The ARGOS satellite was launched 23 February 1999 from Vadenberg AFB aboard a Delta II into a 97 degree near-polar orbit at 846 km altitude. The ESEX contamination diagnostics were powered up to receive data on orbit 1.4 (1 hr 25 min after launch). The TQCMs were powered up and commanded to cool on orbit 5.1 (8 hrs 14 min after launch) to enable measurements of the spacecraft outgassing during the vehicle initialization and check-out. A total of eight ESEX firings were performed between 15 March 1999 and 21 April 1999. A summary of the ESEX events related to the contamination measurements is shown in Table 2.

A. TQCM Measurements

The TQCM mass deposition recorded from shortly after launch through the battery anomaly is shown in Fig. 4. Each of the TQCMs show a rapid rise shortly after launch that decays in time, indicative of a decreasing outgassing rate from the spacecraft. Bake-off events, denoted by the vertical dashed lines, correspond to times when the TQCM sensors are commanded to heat and vaporize off collected mass. Sunsafe modes of the satellite are accompanied by a data drop out and typically a decrease in the total mass deposition. The mass decrease is attributable to the TQCM temperature rising with the loss of power during the sunsafe event, resulting in a material bake-off. TQCM #4 starts the flight with a mass deposition rate that is likely the best indicator of the spacecraft cleanliness since the sensor is directed towards the spacecraft surface prior to boom deployment. After boom deployment, when the sensor faces the spacecraft ram direction, the mass deposition decreases presumably a result of atomic oxygen interactions with the collected material.

Not surprisingly, the TQCMs show a strong response to the battery anomaly. TQCM #3 exhibits a strong increase in deposition rate. TQCM #1 shows a discreet jump in mass collected through the event. TQCM #2 also shows a dramatic increase in both mass deposition and the deposition

rate. Interestingly, TQCM #2 exhibits a higher deposition rate several days in advance of the anomaly and, in retrospect, may have been a precursor to the event.

Figure 4 shows no large changes in the mass deposition as a result of the arcjet firings, denoted by the vertical lines. This is shown in greater detail in Fig. 5 where the data from each TQCM is shown through the 6 primary firings (duration > 1 min.). TQCM #1 (located on the witness tower and viewing the arcjet nozzle) shows a 140 ng/cm^2 jump in mass deposition with the first firing (F-1C, 141 sec.). Since similar jumps are not apparent on the subsequent firings (F-2 through F-6), this jump is attributed to the first firing of the arcjet as opposed to being an indicator of contamination resulting from steady-state operation.

The subsequent firings on TQCM #1, and the firings on the other TQCMs with a direct view of the arcjet plume, #3 and #4, show a sharp decrease in mass deposition followed by a faster rate of collection that lasts for about 1 day. This period of increased deposition rate is coincident with a rise in the local base temperature apparent on nearby radiometers (not shown). TQCM #2, shielded by the arcjet thermal shield shows no decrease from the firings but does exhibit the 1-day period of increased deposition following each firing.

A detailed plot of the TQCM response to the arcjet firing is shown in Fig. 5 for the 8-minute firing on Day 82. With the arcjet firing, TQCMs with a direct view of the plume (#1, 3, 4) exhibit a prominent short-duration, downward spike and then remain depressed in value until the arc is extinguished. Following the discharge the TQCM returns to its normal solar cycle, albeit at a lower value frequency for TQCMs #1, 3, 4. TQCM #2, blocked by the thermal shield, again shows no significant response to the firing.

B. Solar Cell Segment Measurements

Figure 6 shows the solar cell voltage and current during the six successful arcjet firings. During these firings, the current is seen to rise above zero about ~~two~~ minutes after arcjet start, reaching a nearly equilibrium value in an additional ~~two~~ minutes, and dropping rapidly to zero after arcjet shutdown. This is consistent with illumination of the solar cells with radiation from the arcjet body, as the latter heats to the point of incandescence during operation. Solar cell voltage also follows the same general pattern during the three firings which occurred during eclipse, with the voltage rise occuring slightly earlier, and the post-shutdown dropoff substantially slower, than is observed for the current. Voltage is also observed to drop off slightly during the near-equilibrium phase of the longer firings. As solar cell voltage drops with increasing cell temperature; this is unsurprising.

Two other anomalies are also observed during these firings. At the very beginning of the first two firings, for about ~~twenty~~ seconds after ignition, there is a small voltage spike peaking at about ~~one~~ volt. Also, immediately after shutdown there is a small, instantaneous jump in voltage, after which the voltage trails off as the arcjet cools. The magnitude of this jump increases from approximately 0.2 volts after the first firing to 0.6 volts after the last in the sequence.

Slightly different behavior is seen on the three firings which occurred while the solar cells are exposed to indirect sunlight – the spacecraft being in sun, but the solar cells shadowed by the arcjet heat shield and/or the ESEX package deck. In this geometry, the solar cells receive enough illumination due to sunlight scattered or reflected from other components of the spacecraft to maintain a steady-state open circuit voltage of 2-3 volts, but no measurable current. The 8/33/99 firing occurred less than ~~two~~ minutes after the solar cells went into shadow, resulting in a brief interval of high current and voltage unrelated to the arcjet firing being observed in the data.

Solar cell current during these firings followed the same pattern as with the eclipse firings. So to did solar cell voltage after the first ~~two~~ minutes of the firing, with the obvious exception of falling off to the original

steady-state voltage due to indirect illumination, rather than to zero, after shutdown. The instantaneous post-shutdown jump is observed in these firings, again increasing in magnitude with each successive firing.

The substantial difference between the indirect-illumination firings and the eclipse firings is in the behavior of the solar cell voltage during the first ~~two~~ 3 minutes. In all three cases, the voltage begins to fall off from the original steady-state value about ~~forty~~ 40 seconds into the firing, and drops precipitously at about ~~sixty~~ 60 seconds. Voltage recovers equally rapidly about ~~ten~~ 10 to ~~twenty~~ 20 seconds later, shortly before the current rise and at approximately the time the voltage is observed to rise from zero in the eclipse firings. Both the magnitude and duration of the voltage transient increase in successive firings.

In light of the observed effect of arcjet operation on solar cell voltage, it may be instructive to examine the V-I curve for the solar cells with the arcjet in both on and off states. The illumination of the solar cells by the incandescent arcjet body, which continues for some time following arcjet shutdown, offers an opportunity for such a comparison, and Figure 7 shows voltage vs. current data for all six full-length arcjet firings. With the arcjet shut down, all available data falls on a single curve, and even immeasurably small currents correlate with open-circuit voltages in excess of 3 volts. When the arcjet is operating, however, the V-I curve is shifted down in voltage from the arcjet-off case, with the magnitude increasing at each firing. The shift is most pronounced for low current values, and much less significant at currents of 10 mA or greater. This is consistent with the observed voltage jump following arcjet cutoff, and may help explain the voltage drop at ~~sixty~~ 60 seconds after ignition in the partial-illumination cases.

C. Radiometer Measurements

Figure 8 shows the measured sensor head temperature at all four radiometers during the 3/23/99 arcjet firing. At ~~eight~~ 8 minutes, this was the longest arcjet firing of the ESEX experiment. As can be seen, radiometers #1 and #2 both show a steady increase in temperature throughout the course of the firing. However, other observations, particularly video images and solar cell performance measurements, indicate that radiant emissions from the arcjet remain nearly constant after the first two or three minutes of operation. In addition, the arcjet itself is expected to reach thermal equilibrium in that period.

This discrepancy suggests that the radiometers themselves are not reaching thermal equilibrium in the course of an ~~eight~~ 8-minute firing. Notwithstanding the small size, and thus heat capacity, of the witness plates, the decision to minimize heat transfer away from the plate to increase the precision of the measurements has the unfortunate effect of increasing the equilibration time of the system. Experiments with identical radiometers on the ground subject to constant radiation flux show a constant rise in sensor head temperature over ~~five~~ 5 minutes of constant exposure.

Figure 9 shows the behavior of the radiometers over a period of several days at three points in the mission – prior to any arcject firing, after the first seven firings totaling approximately ~~thirty~~ 30 minutes of operation, and after the battery failure at the end of the ESEX experiment. For radiometer #1, with the greatest exposure to the arcjet plume, a significant effect is seen. The radiometer base temperature varies in a constant fashion from a minimum of 260±2 K in eclipse to 271±2 K in direct sunlight. Prior to arcjet operation, the sensor head shows a broader range of temperatures, from 253±2 K in eclipse to 275±2 K in direct sunlight. This indicates that the sensor head is radiating heat when in shadow and absorbing heat in sunlight, as expected.

However, following the arcjet firings, the maximum temperature in direct sunlight increases to 279±1 K, essentially doubling the temperature differential across the radiometer. As the temperature difference across the radiometer is roughly linear with incident heat flux, and the intensity of solar radiation is of course constant, this indicates a doubling of the solar absorbtivity of the radiometer surface material. The minimum temperature of the radiometer during eclipse is unchanged, indicating that the IR emissivity of the surface is not altered by exposure to the arcjet operating environment. Following the battery failure event, another, modest increase in maximum sensor head temperature to 280±1 K is noted, with the minimum temperature again unchanged.

Radiometers 2 and 3, being limited in their exposure to the arcjet plume and to incident solar radiation by the arcjet heat shield, show no significant changes during the ESEX mission. Radiometer #4 shows a smaller but still noticeable increase in sensor head temperature following arcjet firings, and a much larger increase following the battery failure. As radiometer #4 is mounted farther from the arcjet and closer to the batteries this is unsurprising.

IV. Discussion

With each firing TQCMs #1,3,4 show a pronounced decrease in mass deposition. Since these sensors have a view of the arcjet plume, whereas obscured sensor #2 shows no effect, two likely causes are the radiative impingment from the plume or the expulsion of reactive species from the plume that act to remove deposited mass. For radiative impingement, one would expect the effect to scale with distance from the thruster exit. In that event the effect should be most pronounced for sensor #1, followed by sensors 3, and 4. By contrast the data shows the effect to approximatly equal for sensors 3 and 4 suggesting that the cause is the expulsion of reactive specie from the arcjet.

Following each firing each TQCM exhibits a marked increase in the deposition rate for about 1 day. Similarly the temperature in the region of each sensor increases on about the same time scale. The cause of the increased deposition rate is believed to an elevated rate of surface outgassing due to the elevated temperatures. In support of this conjecture, after each TQCM bake-out an increased deposition rate is also observed while the TQCM is cooled back down to it's operational temperature. The peltier heater/coolers within the TQCMs have the effect of heating the local area while cooling the TQCM sensor. Thus the increased deposition rate after a bake-out is also attributed to an enhanced outgassing rate due to a temporary local increase in the spacecraft temperature. Fully analyzed, this data may be valuable in determining to what extent outgassing can be reduced through thermal designs that act to keep localized areas of the spacecraft at reduced temperatures.

The only mass deposition increase observed in conjunction with a firing occurs on TQCM #1 after the first firing. This increase is not observed on subsequent firings that are both longer then and shorter than Firing 1. The increase is believed to be material left in the arcjet during the fabrication, assembly, and integration process that ejects during the first firing. It is not believed to be indicative of contamination associated with steady-state arcjet operation.

Degradation in the solar cell voltage is believed to be a result of the plasma forming an alternate, shorting current path. The effect is observed to increase with successive firings possibly due to insulator erosion at the short increasing the effective area of the plasma current connection site. This effect is believed to be indicative of plasma exhaust impingement on a solar array and should be avoided in a full-scale flight design. It should be noted that the main ARGOS solar arrays, well in the backfield of the arcjet, reported no degradation of power during arcjet firings. This indicated that the problem can be alleviated through judicious choice of spacecraft design.

Initial data evaluation indicates a change in the radiative properties of the coating on radiometer #1 with a direct view of the arcjet exhaust. Whereas this may be a very important result for spacecraft designers, a decisive conclusion is beyond the scope of this initial data presentation. A full thermal analysis including transient effects must be incorporated to accurately determine changes in the heat flux into the radiometer over time. It is interesting to note, however, that radiometers 2,3, and 4 with a lesser expected heat flux from the arcjet show no signs of possible

Use of # before 1, 2, 3, 4 is inconsistent in paper, tables and figures.

degradation. Of course, this result must also be tempered with the present lack of a complete thermal analysis of the data.

V. Summary and Conclusions

A preliminary analysis of the data from the ESEX flight is performed to provide an initial assessment of the contamination associated with the use of the 30-kW arcjet. No material deposition is observed for surfaces held at 218K. Indeed, firing the arcjet appears to have the beneficial effects of removing deposited material, presumably through the expulsion of reactive species. Countering this, the thermal heat load from firing the 30-kW thruster leads to an elevated spacecraft temperature which increases the outgassing rate, and hence the material deposition. The latter effect can be tempered through improved thermal design.

Solar cell segments show a decrease in output voltage when the arcjet is fired, presumably due to the formation of an alternate conducting path through the exhaust plasma. This deleterious effect can be controlled through the judicious placement of the thruster relative to the solar arrays.

Initial evaluation of radiometer data suggests material degradation of the S13-GLO coating only for the radiometer nearest the exhaust plume. Further transient analysis of the thermal dynamics is required for a conclusive statement.

Table 1: Locations of Contamination Sensors Relative to Arcjet Exhaust Plane

	Distance (cm)	Angle (degrees)	Sensor Angle (degrees)	
Solar Cells	43	3	42	
TQCM 1	40	-11	79	
TQCM 2	45	-60	60	Under radiation shield
TQCM 3	59	-40	40	
TQCM 4	93	-19	19	On deployable boom
Radiometer 1	40	-11	79	
Radiometer 2	48	-37	53	
Radiometer 3	45	-60	60	
Radiometer 4	60	-41	41	

Table 2: Contamination Events during ESEX Flight Experiment

Firing (F) or Event	Date/Time (Zulu)	Julian Date	Duration
Boom Deployed	09MAR99 14:59:57	68.62497	
F-1C	15MAR99 21:55:55	74.91383	2 m, 21 s
F-2	19MAR99 22:32:23	78.93916	5 m, 1 s
F-3	21MAR99 12:24:41	80.51714	5 m, 33 s
F-4	23MAR99 21:27:57	82.89441	8 m, 2 s
F-5	26MAR99 12:45:25	85.53154	6 m, 4 s
F-6	31MAR99 13:05:37	90.54557	4 m, 29 s
F-7	02APR99 22:09:03	92.92295	53 s 38 s
F-8	21APR99 12:22:12	111.51542	42 s
Battery Anomaly	22APR99 15:18:37	112.63793	

[1] D.R. Bromaghim, et al., "An Overview of the On-Orbit Results from the ESEX Flight Experiment," AIAA paper 99-2706, June 1999.
[2] B.J. Turner, and F.J. Agardy, "The Advanced Research and Global Observation Satellite (ARGOS) Program," AIAA paper 94-4580, Sept. 1994.
[3] B.E. Wood, et al., "MSX Satellite Flight Measurements of Contamination Deposition on a CQCM and on TQCMs," AIAA paper 97-0841, January 1997.

[4] R.J. Bryson, et al., "MSX Thermoelectric Quartz Crystal Microbalances – Calibration and Characterization," 1994 SPIE Intl Symposium, Optical Systems Contamination: Effects, Measurements, and Control IV, Paper No. 2261-25, San Diego, Ca 1994.

[5] D.A. Wallace and S.A. Wallace, "QCM Research Operating Manual – Mark 10," QCM Research, Laguna Beach, CA 1996.

A) Top View

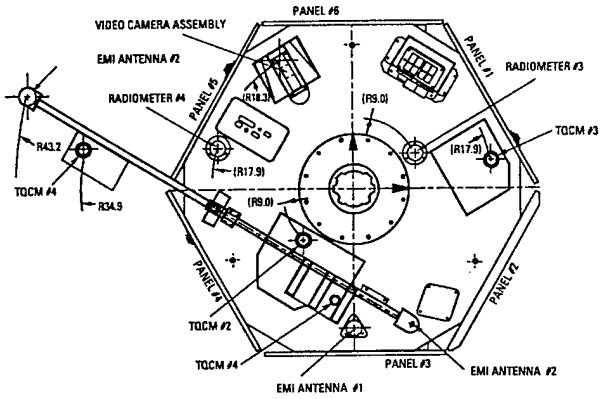

B) Side View

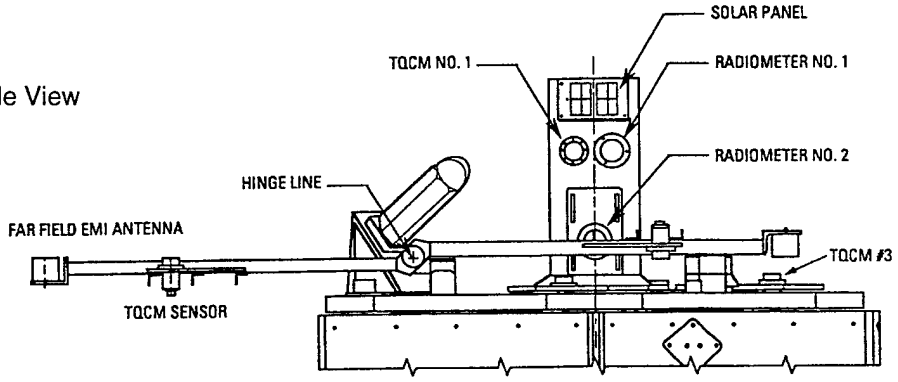

Fig. 1 (A) Top view and (B) Side view of ESEX showing the locations of the contamination sensors.

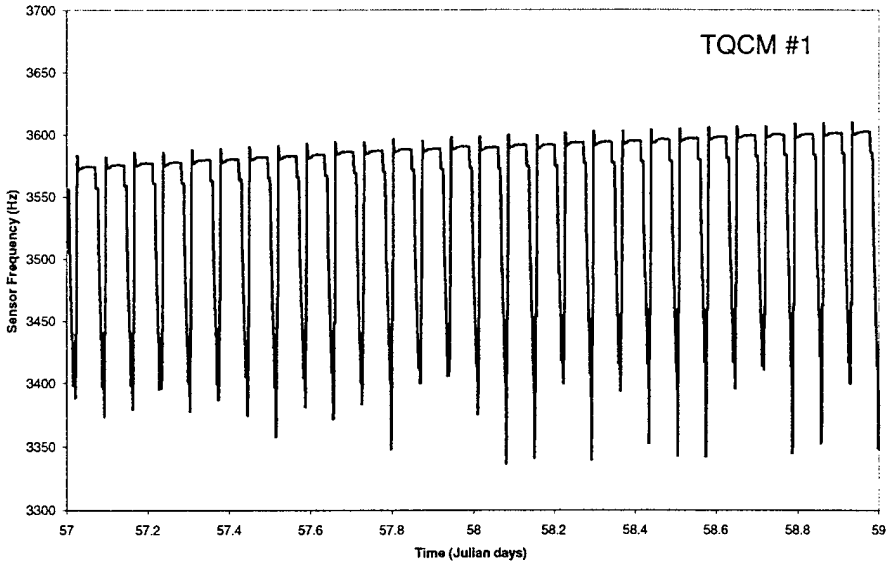

Fig. 2 Representative TQCM data showing the slow frequency increase due to mass deposition superimposed on the larger solar cycle.

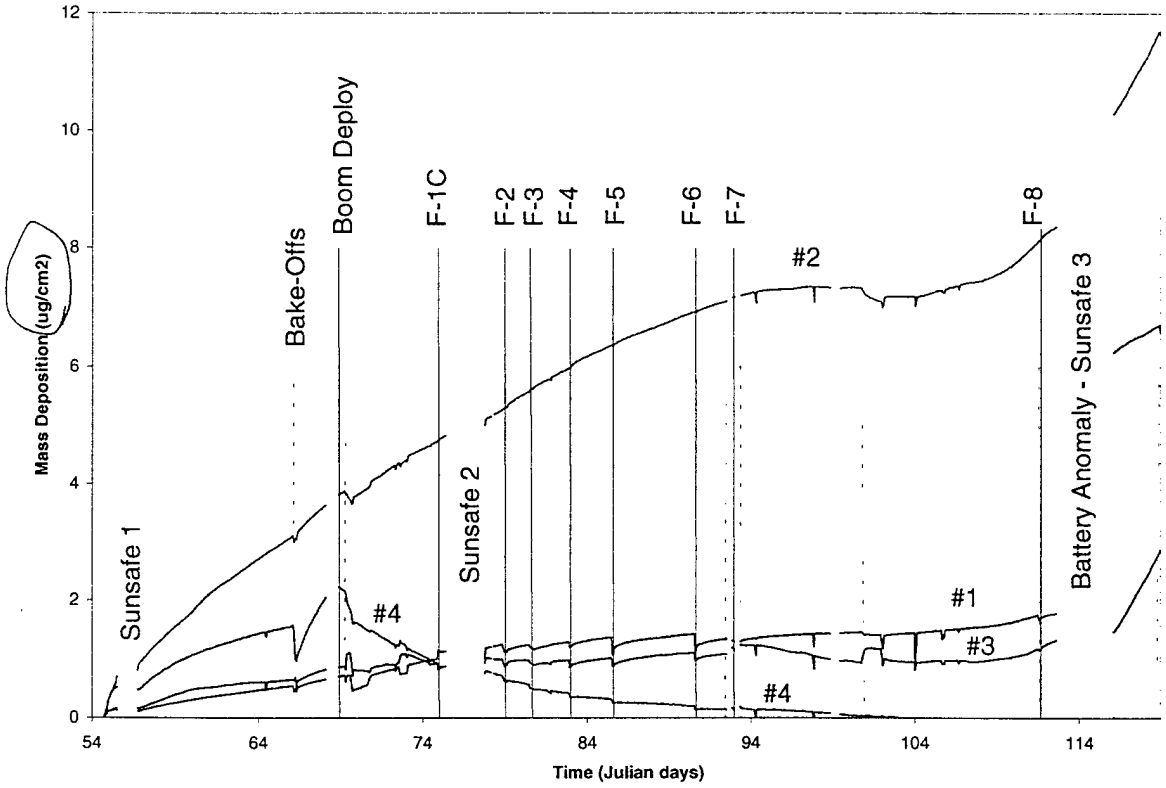

Fig. 3 TQCM behavior from launch through the battery anomaly.

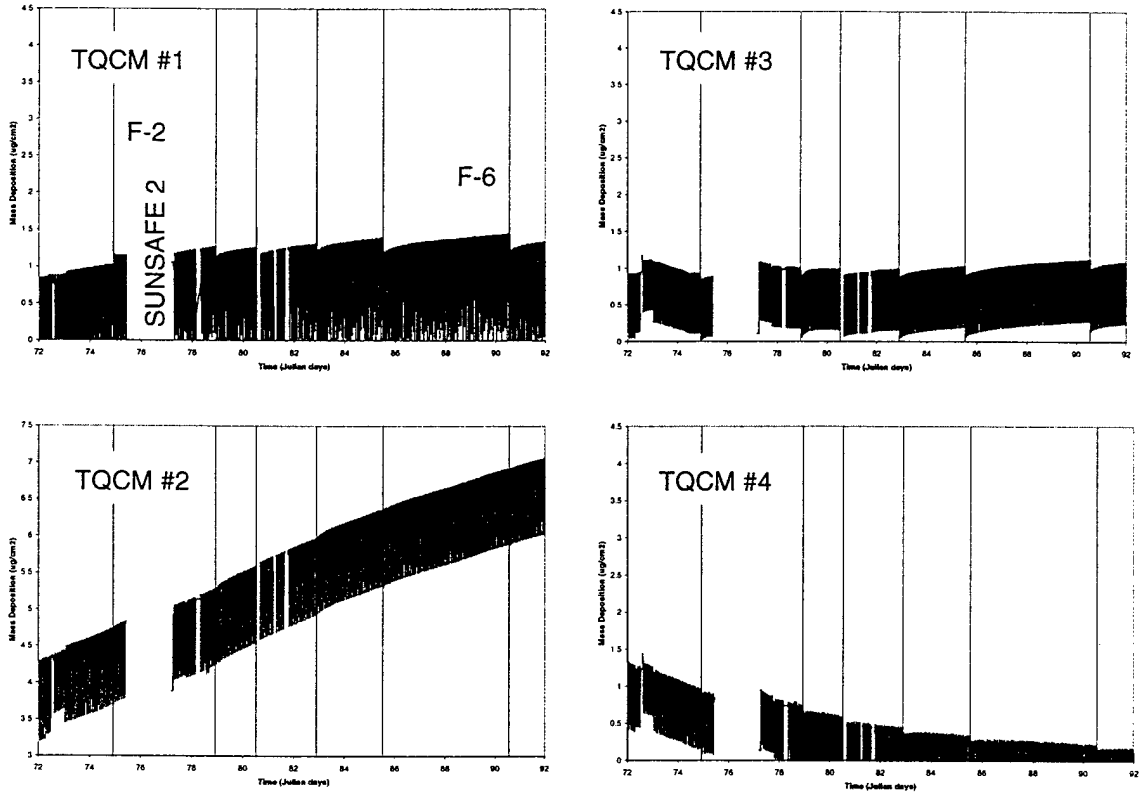

Fig. 4 Mass deposition measured on each of the 4 TQCMs through the primary (6) ESEX firings.

Unable to read axes labels.

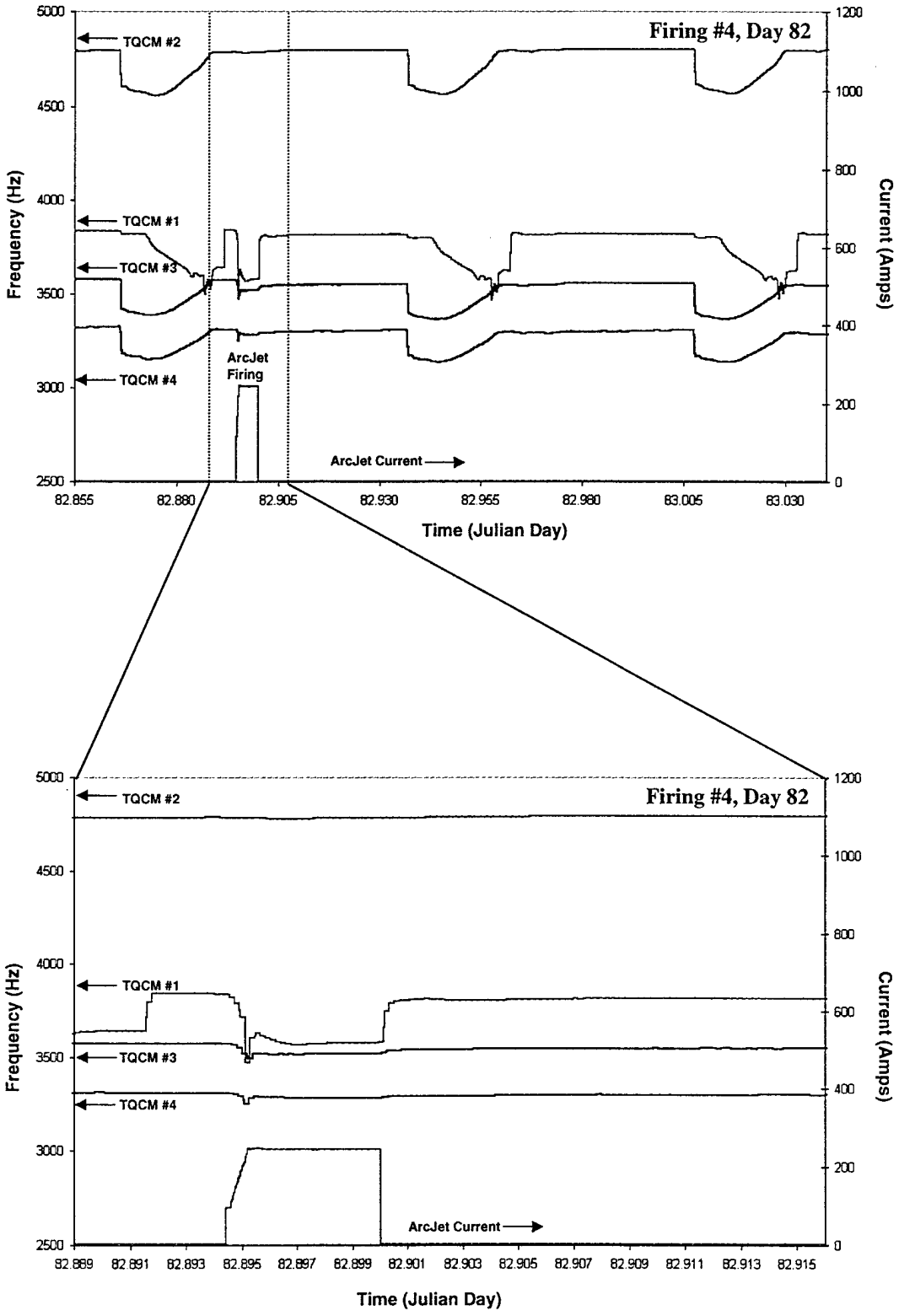

Fig. 5 TQCM response during an ESEX firing

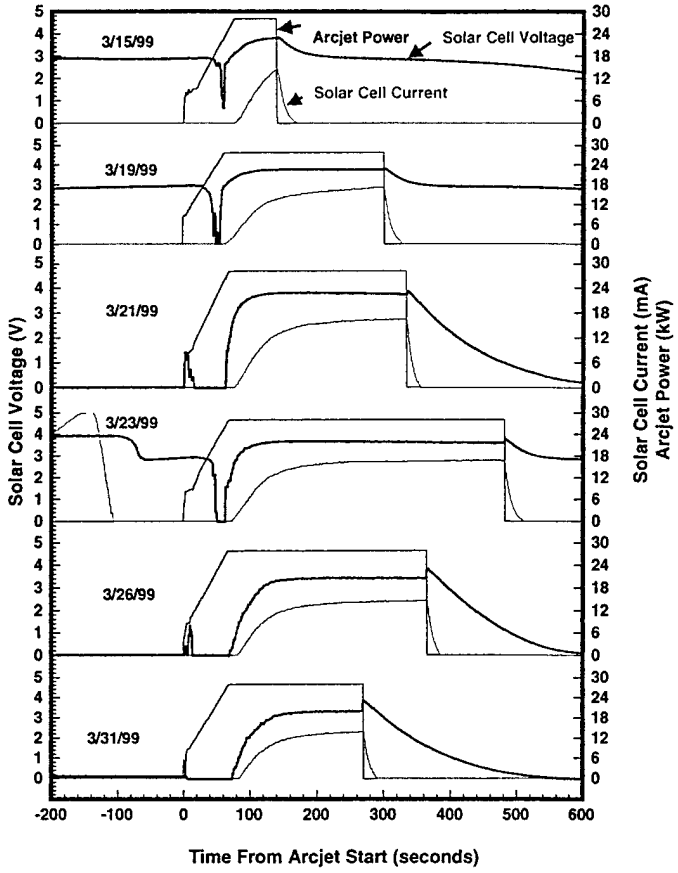

Fig. 6 Solar Cell response to the 6 primary ESEX firings

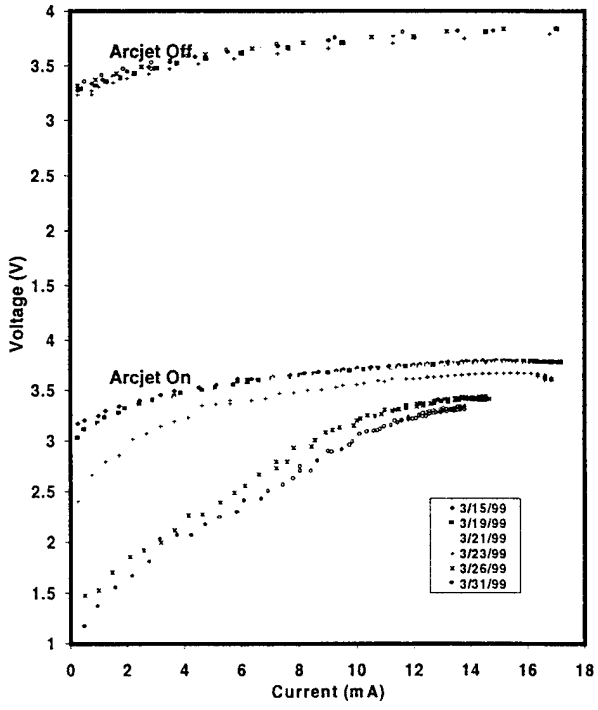

Fig. 7 Solar Cell IV curves during the ESEX firings

In paper referred to as V-I curves.

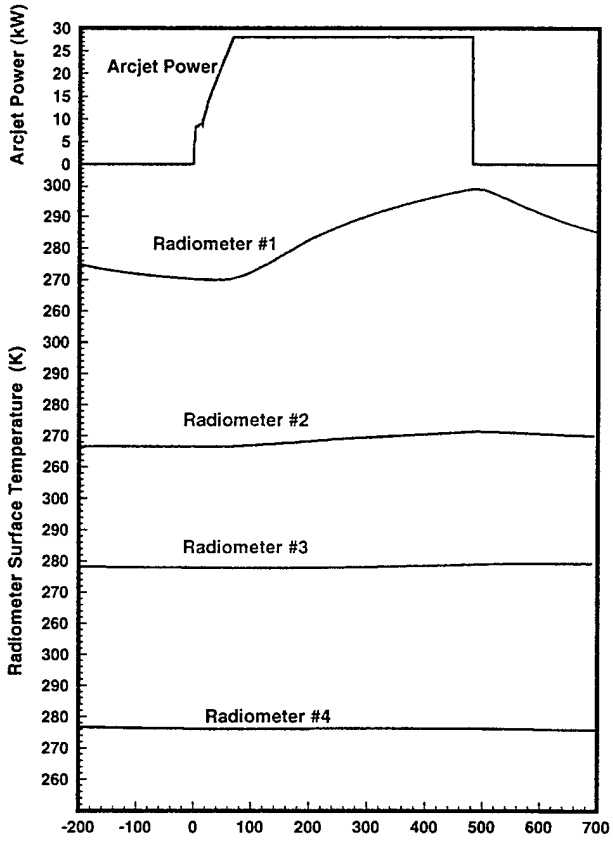

Fig. 8 Radiometer response to an ESEX firing

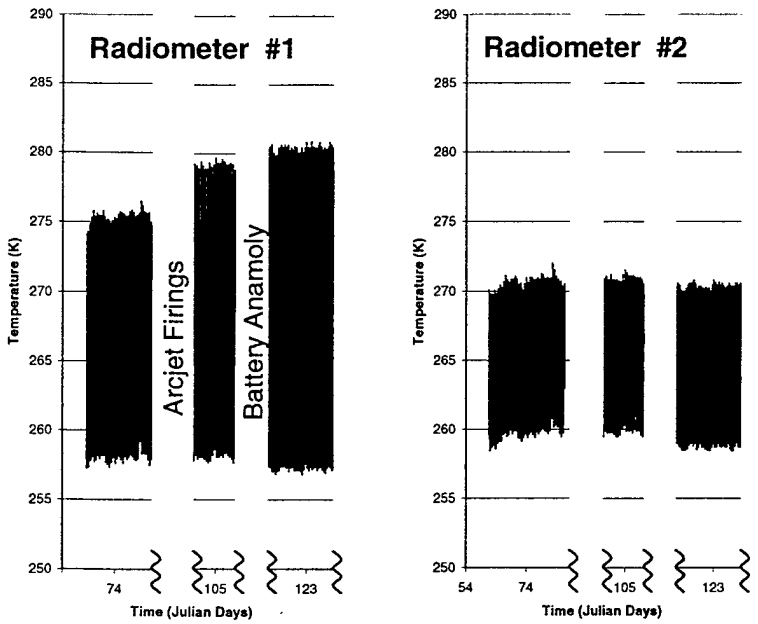

Fig. 9 Changes in the Radiometer response to solar illumination sampled during the flight.